INSTITUTE OF PHYSICS PUBLISHING JOURNAL OF PHYSICS: CONDENSED MATTER

J. Phys.: Condens. Matter **14** (2002) 5609–5618 PII: S0953-8984(02)33169-2

Magnetoelastic effects in $ErNi_2B_2C$ single crystal: probing the H–T phase diagram

M Doerr[1], M Rotter[1], M El Massalami[2], S Sinning[1], H Takeya[3] and M Loewenhaupt[1]

[1] Institut für Angewandte Physik, Technische Universität Dresden, D-01062 Dresden, Germany
[2] IF-UFRJ, CxP68-528, 21945-970 Rio de Janeiro, Brazil
[3] National Institute for Materials Science, Tsukuba, Ibaraki 305-0047, Japan

E-mail: doerr@physik.tu-dresden.de

Received 29 January 2002
Published 23 May 2002
Online at stacks.iop.org/JPhysCM/14/5609

Abstract

Using a capacitive dilatometer we investigated the magnetoelastic behaviour of single-crystalline $ErNi_2B_2C$ in the temperature range 1.8 K $\leqslant T \leqslant$ 16 K and for external magnetic field in the tetragonal ab-plane $\mu_0 H \leqslant 6$ T. For $T \leqslant T_N = 6.4$ K the longitudinal magnetostriction coefficient is negative, whereas the transverse one is positive. The thermal evolution of the lattice distortion $\varepsilon^{\gamma} = (\lambda_{\perp} - \lambda_{\parallel})/\sqrt{2}$ is in agreement with that of the previously reported spontaneous tetragonal-to-orthorhombic distortion determined by neutron diffraction. The behaviour is influenced by the distribution of the magnetic domains in the crystal. The H–T phase diagram, constructed from the magnetostriction curves, shows the well-known cascade of metamagnetic transitions between several phases (antiferromagnetic AF1, ferrimagnetic F1, F2) in the field range $0 < \mu_0 H < 2.1$ T below T_N. On the basis of a Hamiltonian consisting of an exchange, a crystal-field, a Zeeman, and a magnetoelastic term, we were able to reproduce reasonably well the H–T phase diagram as well as various forced magnetostriction curves.

(Some figures in this article are in colour only in the electronic version)

1. Introduction

Among the extensively investigated quaternary borocarbides RNi_2B_2C (R = rare earth) much interest has been focused on $ErNi_2B_2C$ because it shows a wide variety of physical phenomena that are connected with the complex interplay between electronic, magnetic, and lattice properties [1–9]. The compound crystallizes in a body-centred tetragonal structure (space group $I4/mmm$) and becomes superconducting at the critical temperature $T_c = 11.0$ K. The onset of the long-range magnetic order occurs at a lower temperature $T_N = 6.4$ K. Below the

Néel temperature in zero field an incommensurate, transversely polarized sinusoidal magnetic structure was observed by neutron measurements [2, 3]. Two kinds of domain are possible, one with the spins aligned parallel to the [0 1 0] direction with the incommensurate wavevector $\boldsymbol{q} = (0.5586, 0, 0)$, the other with spins parallel to the [1 0 0] direction and $\boldsymbol{q} = (0, 0.5586, 0)$.

The H–T phase diagram of $ErNi_2B_2C$ was investigated by means of neutron diffraction [6], magnetization [5], and magnetoresistivity [5]. The phase diagrams for various field orientations such as [1 0 0], [1 1 0], and [0 0 1] exhibit a complex character and show the existence of at least three magnetic phases for fields in the tetragonal plane. All magnetic phases are described as incommensurate states with slightly different propagation vectors. A weak ferromagnetic component in the zero-field phase below $T_{WF} \approx 2.2$ K was reported in [7]. In contrast, the authors of [6] observed a small ferromagnetic component in the ferrimagnetic phase F1 only above $\mu_0 H = 1$ T. Besides the analysis of the long-range magnetic order in $ErNi_2B_2C$, synchrotron x-ray scattering experiments revealed a tetragonal-to-orthorhombic lattice distortion below T_N [8]. The value of $|a/b - 1|$ is about 0.2% at 3.7 K. The distortion in zero magnetic field and its relation to the magnetic ordering has been studied also, in [9].

In the present study, magnetostriction and thermal expansion measurements were carried out in order to evaluate in more detail the magnetic H–T phase diagram as well as the magnetoelastic interactions. Of particular interest is checking the ability of macroscopic magnetostriction techniques to reveal the reported lattice distortion. Furthermore, the stability of the metamagnetic phases has been investigated by means of time-dependent relaxation measurements.

2. Experimental details

The $ErNi_2B_2C$ single crystals were grown by the floating zone method [10, 11]. The samples used for our investigations were cut out of the same boule as the ones used in an earlier unpolarized neutron diffraction study [7] and in zero-field specific heat measurements [12]. The good quality of the single crystal was checked by extensive structural, resistive, thermal, and magnetic characterizations (for details see [7, 12]).

For the magnetostrictive measurements a small single-crystalline piece ($1.3 \times 2.4 \times 1.0$ mm^3) was mounted between the capacitor plates of a compensated miniature dilatometer [13]. This device allows one to measure both longitudinal $\lambda_\parallel = (\Delta l/l)_\parallel$ and transverse $\lambda_\perp = (\Delta l/l)_\perp$ magnetostriction because the capacitor may be adjusted parallel or perpendicular to the external-field direction. The measurements were performed in an Oxford Instruments MagLab low-loss cryostat (temperature range $T = 1.5$–300 K) equipped with a 14 T superconducting magnet. Isothermal (=forced) magnetostriction was measured by ramping the field between 0 and 10 T with a rate of 0.2 T min^{-1}. Thermal expansion at various fixed fields was measured by sweeping the temperature from 12 K (or from 16 K in some experiments) to 1.8 K with a rate of 0.3 K min^{-1}. Between several scans the sample was heated up well above T_N and subsequently cooled down in zero field to avoid the freezing in of ordered states.

External magnetic fields were applied either along the [1 0 0] or the [0 1 0] direction. Equivalent behaviours along the two directions are expected for a tetragonal system.

3. Results and discussion

The relative changes in sample length, $\lambda_\parallel$ and $\lambda_\perp$, obtained from thermal expansion and magnetostriction measurements are plotted in figure 1 for fields along the [1 0 0] direction and

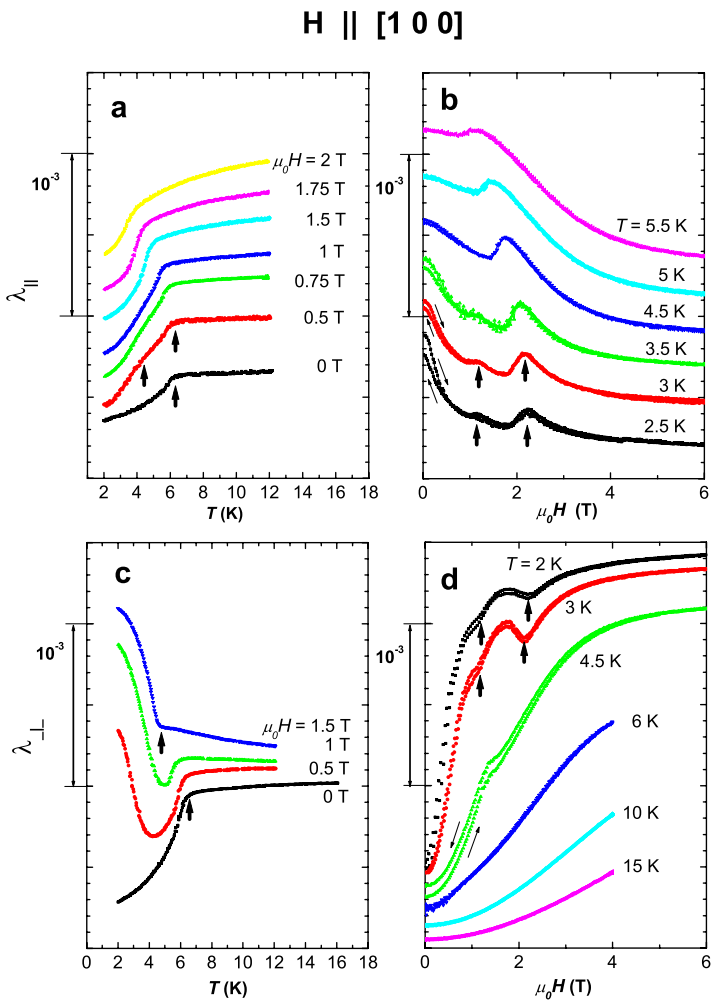

Figure 1. Thermal expansion (parts (a), (c)) and forced magnetostriction (parts (b), (d)) behaviour of an $ErNi_2B_2C$ single crystal in external magnetic fields aligned in the ab-plane parallel (parts (a), (b)) and perpendicular (parts (c), (d)) to the crystallographic [1 0 0] direction. (The scales of the vertical axes are equal for all diagrams.) Some phase transition points used for the construction of the H–T phase diagram (figure 3) are marked by arrows as an example.

in figure 2 for fields along the [0 1 0] direction. The data illustrate the strong anomalies at the ordering temperature connected with the transition from the paramagnetic into the magnetically ordered state. The Néel temperature of the compound is $T_N = 6.4$ K in accordance with earlier studies. In all thermal expansion curves, there was no detectable change in the sample length at the superconducting critical point, indicating that the contribution of superconductivity to the magnetostriction is below our experimental resolution.

The thermal expansion curves in zero field are characterized by small changes of the sample length for $T > T_N$. Below T_N there are pronounced changes of the sample length with temperature. Note that in figure 1 the zero-field longitudinal expansion between low temperatures and T_N is much less than the transverse one ($\Delta\lambda_{\parallel} = 2.9 \times 10^{-4}$, $\Delta\lambda_{\perp} = 6.8 \times 10^{-4}$), whereas in figure 2 the situation is inverted ($\Delta\lambda_{\parallel} = 7.0 \times 10^{-4}$, $\Delta\lambda_{\perp} = 0.85 \times 10^{-4}$).

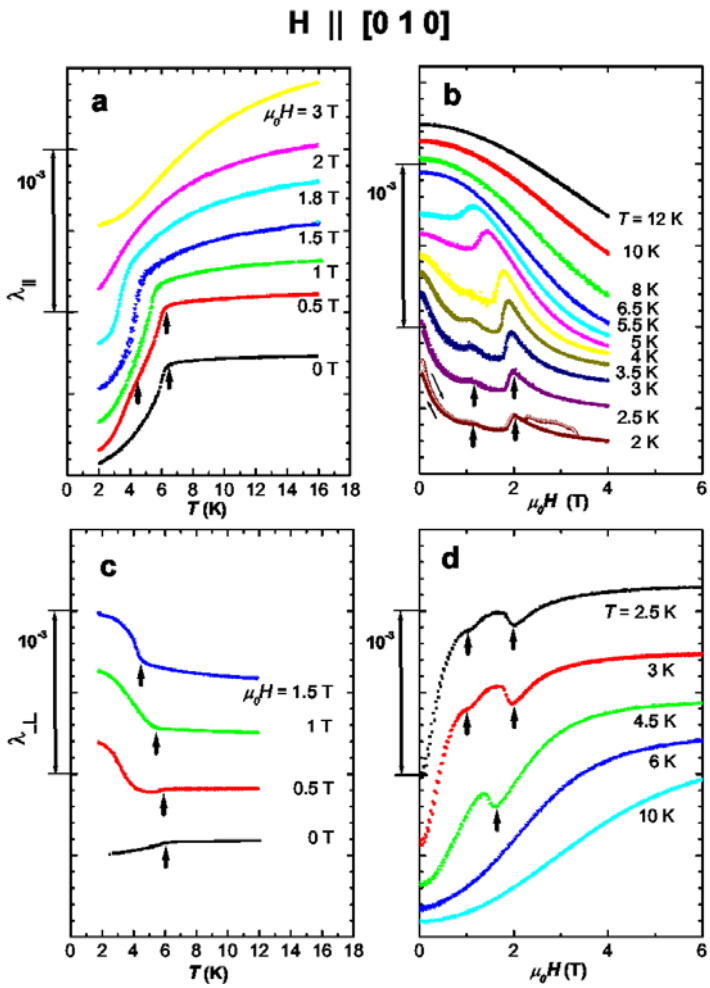

Figure 2. Thermal expansion (parts (a), (c)) and forced magnetostriction (parts (b), (d)) behaviour of an $ErNi_2B_2C$ single crystal in external magnetic fields aligned in the *ab*-plane parallel (parts (a), (b)) and perpendicular (parts (c), (d)) to the crystallographic [0 1 0] direction, (The scales of the vertical axes are equal for all diagrams.) Some phase transition points used for the construction of the H–T phase diagram (figure 3) are marked by arrows as an example.

This anisotropy constitutes clear evidence that the domains in the tetragonal plane are not equally distributed. Taking into account the tetragonal to orthorhombic lattice distortion below T_N with relative changes of the lattice parameters from low temperatures up to T_N of about $\Delta a/a \cong -1.1 \times 10^{-3}$, $\Delta b/b \cong +1.0 \times 10^{-3}$ [8], the relative populations of domains with moments along the [1 0 0] and [0 1 0] directions were estimated to be approximately 35 and 65%, respectively.

Thermal expansion measurements in finite magnetic fields (figures 1(a), (c) and 2(a), (c)) show distinct features for $T < T_N$. On increasing the temperature the sample expands parallel to the external field ($\Delta\lambda_{\parallel} > 0$) and contracts perpendicular to the field ($\Delta\lambda_{\perp} < 0$). The transverse thermal expansion curves for fields along [1 0 0] (see figure 1(c)) have a pronounced minimum due to the higher amount of domains with moments along [0 1 0] which

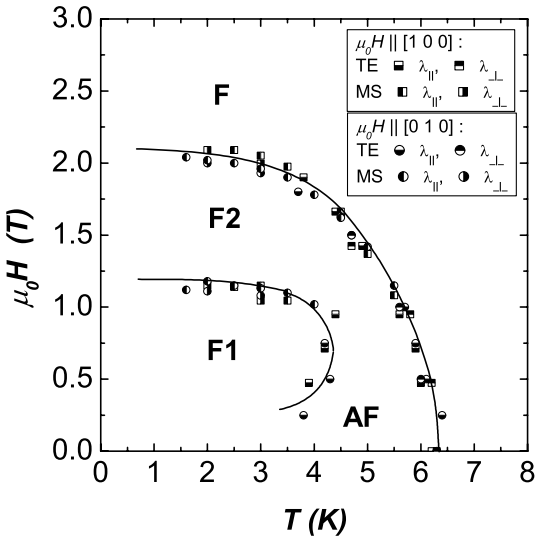

Figure 3. The magnetic phase diagram of $ErNi_2B_2C$ for external magnetic fields parallel to the crystallographic [1 0 0] and [0 1 0] directions as constructed from capacitive dilatometric measurements. (The symbols denote the kind of measurement and (TE = thermal expansion, MS = magnetostiction) the direction of the measurement in comparison with the field direction.)

tend to contract the sample when decreasing the temperature below T_N. For the other direction (figure 2(c)) the minimum has nearly vanished. Going to higher fields, the anomaly connected with the onset of the magnetic order vanishes above 2 T (see figures 1(a) and 2(a)) and the sample reaches the ferromagnetically aligned state F3.

The field-induced length variations are manifested in the forced magnetostriction isotherms shown in figures 1(b), (d) and 2(b), (d). First, the curves for the two crystallographic directions investigated are not different from each other: the value of the field-induced longitudinal magnetostriction $\Delta\lambda_{\parallel}$ is negative (i.e. the sample contracts with increasing field) and the transverse magnetostriction $\Delta\lambda_{\perp}$ is positive, for fields along the [1 0 0] direction as well as for the [0 1 0] direction. Second, for field values above 2.2 T the curve shape is monotonic; the sample lengths stay almost unchanged as expected for a saturated state. Third, when the magnetic field is brought back to zero, the system nearly recovers its initial state (very small hysteresis effects). This shows that a remarkable change of the domain distribution cannot be achieved upon application of an external field $\leqslant$6 T. Finally, below the magnetic ordering temperature T_N all curves are characterized by drastic changes of slope. These anomalies indicate phase transitions between different magnetic states. They vanish at higher temperatures when the sample is in the paramagnetic state and the magnetostriction coefficient is rather small.

Based on the (H, T) anomalies in the measured magnetostriction and thermal expansion curves, the magnetic H–T phase diagram was constructed (figure 3). The phase transition points were taken from bends of the thermal expansion curves, which are characterized by jumps in the derivatives of the experimental curves, or from extrema points in the forced magnetostriction (compare arrows in figures 1 and 2).

In zero field the low-temperature phase AF1 exists over a wide temperature interval and corresponds to the incommensurate phase characterized by $\boldsymbol{q} = (0.55, 0, 0)$ as reported in [2]. However, small bends in the low-field expansion curves were found and give a hint that the

AF1 phase is modified in the temperature range 5.3 K $< T <$ T_N (not shown here). In magnetic fields 0.3 T $< \mu_0 H <$ 2.1 T two magnetic phases are detected, marked by F1 and F2 in figure 3. They contain a ferromagnetic component as found for the phases in measurements parallel to the [1 1 0] direction [6], but the propagation vectors of the magnetic structures are still unknown. The ranges of existence of the phases F1 and F2 agree well with the results reported in [5]. On increasing the field above 2.1 T the sample reaches the induced ferromagnetic state F3. Apart from this clear evidence, the behaviour in the range $T = 4.2$–6.4 K and $\mu_0 H = 0$–1 T is still unclear. Note that the measurements in small magnetic fields consist of contributions of two domains—thus the phase diagram in low fields shows phase boundaries which originate microscopically from the behaviour of the domains (weighted with the field-dependent domain distribution) in a magnetic field applied parallel and perpendicular to the propagation. The phase transition lines in this region could not be detected in detail with any of the macroscopic methods used because of their limited sensitivity. The use of scattering experiments may be helpful to solve this problem.

Moreover, we checked the dynamical stability of this phase diagram by carrying out time-dependent dilatometric measurements at several (H, T) points including those near the phase boundaries. It was observed that the sample lengths maintain their values over a long time period ($t \sim 1$ h) indicating that relaxation effects are negligible in this time window.

4. Theoretical consideration

In addition to the experimental investigations, the main features of the magnetostriction of $ErNi_2B_2C$ have been calculated using the following theoretical model. The Hamiltonian consists of a crystal-field (CF), an exchange (EX), a Zeeman, and an elastic term

$$\mathcal{H} = \mathcal{H}_{CF} + \mathcal{H}_{EX} - \sum_i g_J \mu_B \mathbf{H}_{ext} \cdot \mathbf{J}_i + E_{el}. \tag{1}$$

In order to describe magnetoelastic properties, the strain dependence of the crystal-field part has to be considered. The different terms in (1) can be described by the following expressions (for the notation, see [14]; α and β denote the components of the vectors or tensors, $\boldsymbol{i}$ and $\boldsymbol{j}$ the positions of the Er^{3+} ions):

$$\mathcal{H}_{CF} = \sum_{lm,i} B_l^m(\varepsilon) O_l^m(\mathbf{J}_i) \tag{2a}$$

$$\mathcal{H}_{EX} = -\tfrac{1}{2} \sum_{i,\boldsymbol{j},\alpha,\beta} \mathbf{J}_i^\alpha J^{\alpha\beta}(\boldsymbol{i}-\boldsymbol{j}) \mathbf{J}_{\boldsymbol{j}}^\beta \tag{2b}$$

$$E_{el} = \tfrac{1}{2} \sum_{\alpha\beta\alpha'\beta'} \varepsilon_{\alpha\beta} \varepsilon_{\alpha'\beta'} C^{\alpha\beta\alpha'\beta'}. \tag{2c}$$

In our approach the magnetic order is treated using a mean-field model [15] according to

$$\mathcal{H}_{EX} = -\sum_i g_J \mu_B \mathbf{H}_{MF,i} \cdot \mathbf{J}_i + \tfrac{1}{2} \sum_{i,\boldsymbol{j},\alpha,\beta} \langle \mathbf{J}_i^\alpha \rangle_{T,\mathbf{H}} J^{\alpha\beta}(\boldsymbol{i}-\boldsymbol{j}) \langle \mathbf{J}_{\boldsymbol{j}}^\beta \rangle_{T,\mathbf{H}} \tag{3}$$

with the molecular field ('MF')

$$\mathbf{H}_{MF,i}^\alpha = \frac{1}{g_J \mu_B} \sum_{\boldsymbol{j},\beta} J^{\alpha\beta}(\boldsymbol{i}-\boldsymbol{j}) \langle \mathbf{J}_{\boldsymbol{j}}^\beta \rangle_{T,\mathbf{H}}. \tag{3a}$$

Now, the magnetic phase calculation program *McPhase*[4] has been used to search for stable mean-field spin configurations: the crystal-field parameters B_l^m used in our calculation

[4] *McPhase program* is available at http://www.mcphase.de.

Table 1. Parameters of the exchange tensor of $ErNi_2B_2C$ as estimated from known basic magnetic properties by a *McPhase* (see footnote 1) simulation. The exchange is assumed to be diagonal but anisotropic (bold numbers).

X (a)	Y (b)	Z (c)	J_{aa} (meV)	J_{bb} (meV)	J_{cc} (meV)
+1.0	0	0	**−0.0010**	**−0.0022**	−0.0020
0	+1.0	0	**−0.0022**	**−0.0010**	−0.0020
+0.5	+0.5	+0.5	−0.0014	−0.0014	−0.0014
0	0	+1.0	+0.0030	+0.0030	+0.0030
+1.0	+1.0	0	−0.0020	−0.0020	−0.0020

were taken from [16] (the coordinates x, y, z are chosen parallel to a, b, c, respectively): $B_2^0 = -1.509 \times 10^{-2}$ meV, $B_4^0 = +1.380 \times 10^{-4}$ meV, $B_4^4 = -3.235 \times 10^{-3}$ meV, $B_6^0 = -1.207 \times 10^{-6}$ meV, $B_6^4 = +2.263 \times 10^{-5}$ meV.

The crystal-field ground state of the $J = 15/2$ Er^{3+} ion in $ErNi_2B_2C$ can be described by a quasi-quartet consisting of two doublets separated by an energy interval Δ. In order to accelerate the numerical calculation of complicated magnetic unit cells, the single-ion part of the Hamiltonian

$$\mathcal{H}_i = \mathcal{H}_{CF,i} - g_J \mu_B \mathbf{H}_i \cdot \mathbf{J}_i \qquad \text{with } \mathbf{H}_i = \mathbf{H}_{MF,i} + \mathbf{H}_{ext} \tag{4}$$

(for small effective magnetic fields $\mathbf{H}_i$ in comparison to the crystal field) is treated only within the crystal-field ground-state quasi-quartet. In that special case it can be written as

$$\mathcal{H}_i = \begin{pmatrix} -\Delta/2 & 0 & 0 & 0 \\ 0 & -\Delta/2 & 0 & 0 \\ 0 & 0 & \Delta/2 & 0 \\ 0 & 0 & 0 & \Delta/2 \end{pmatrix} - g_J \mu_B (H_i^a J_i^a + H_i^b J_i^b + H_i^c J_i^c) \tag{5}$$

with the angular momentum operators given by the 4×4 matrices

$$J_i^a = \begin{pmatrix} 0 & B & 0 & C \\ B & 0 & -C & 0 \\ 0 & -C & 0 & E \\ C & 0 & E & 0 \end{pmatrix},$$
$$J_i^b = \begin{pmatrix} 0 & -\mathrm{i}B & 0 & \mathrm{i}C \\ \mathrm{i}B & 0 & \mathrm{i}C & 0 \\ 0 & -\mathrm{i}C & 0 & -\mathrm{i}E \\ -\mathrm{i}C & 0 & \mathrm{i}E & 0 \end{pmatrix}, \tag{5a}$$
$$J_i^c = \begin{pmatrix} A & 0 & 0 & 0 \\ 0 & -A & 0 & 0 \\ 0 & 0 & -D & 0 \\ 0 & 0 & 0 & D \end{pmatrix}.$$

The constants A–E can be computed from the crystal-field parameters given above. The values are $A = -0.4768$, $B = -3.4683$, $C = -3.5791$, $D = -0.4659$, $E = 3.663$, $\Delta = 0.575$ meV.

The exchange parameters $J^{\alpha\beta}$, given in table 1, are the result of a self-consistent estimation using *McPhase* simulations, which were based on a next-neighbour interaction in the a-direction taking into account T_N and the known magnetic structure of $ErNi_2B_2C$ in zero field. Note that it was necessary to introduce an exchange anisotropy to stabilize the transversely polarized magnetic structure. For the refinement of the exchange parameters, neutron scattering experiments in a magnetic field are required.

As a result of the simulation, we find in the magnetically ordered state in zero field a transverse spin wave with a propagation vector of about $\boldsymbol{q} = (0.5, 0, 0)$. Considering that only

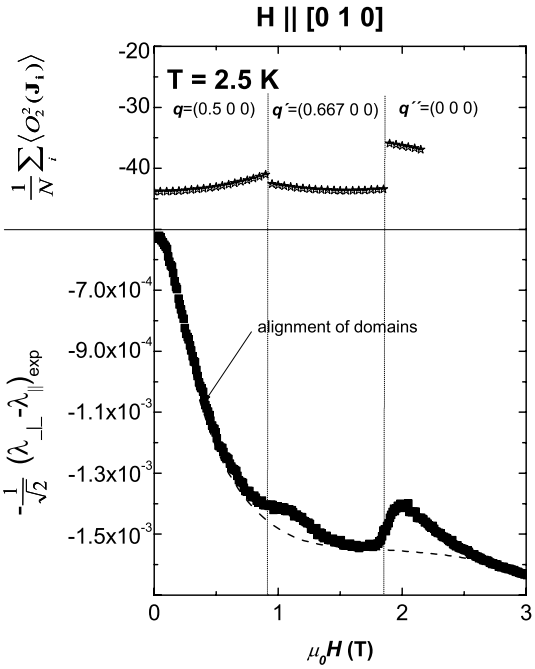

Figure 4. The field dependence of $\sum_i \langle O_2^2(\mathbf{J}_i)\rangle_{T,\mathbf{H}}$ calculated with the magnetic phase calculation program *McPhase* (http://www.mcphase.de) (upper graph) and of the symmetrized strain taken from the experimental data (lower graph). The dotted curve is a guide to the eyes, present to indicate the proposed effects caused by domains at $T = 2.5$ K and at magnetic fields parallel to [0 1 0].

five different exchange constants have been used, this result is in good agreement with the wavevector $\boldsymbol{q} = (0.5586, 0, 0)$ reported in the literature [2] for the zero-field low-temperature phase. For fields in the range 1 T $< \mu_0 H <$ 2 T along the [0 1 0] direction, a transverse spin wave with the propagation vector $\boldsymbol{q}' = (0.667, 0, 0)$ is calculated. This field range corresponds to phase F2.

On the basis of the *McPhase* results we also calculated the magnetostriction by minimizing the total free energy with respect to the strain. The lattice distortion is given in the symmetrized notation of [14] by

$$\varepsilon^{\gamma} = \frac{1}{\sqrt{2}}(\varepsilon_{CF}^{aa} - \varepsilon_{CF}^{bb}) \tag{6a}$$

with

$$\varepsilon_{CF}^{\alpha'\alpha'} = \frac{1}{N}\sum_i (K^{\alpha'\alpha'}\langle O_2^0(\mathbf{J}_i)\rangle_{T,\mathbf{H}} + L^{\alpha'\alpha'}\langle O_2^2(\mathbf{J}_i)\rangle_{T,\mathbf{H}}) \qquad (\alpha' = a, b, c). \tag{6b}$$

Since $K^{aa} = K^{bb}$ for tetragonal symmetry [14], the orthorhombic distortion is proportional to the expectation value $\sum_i \langle O_2^2(\mathbf{J}_i)\rangle_{T,\mathbf{H}}$:

$$\varepsilon^{\gamma} = \frac{1}{\sqrt{2}N}(L^{\alpha\alpha} - L^{\beta\beta})\sum_i \langle O_2^2(\mathbf{J}_i)\rangle_{T,\mathbf{H}} = \frac{B^{\gamma}}{C_0^{\gamma}}\frac{1}{N}\sum_i \langle O_2^2(\mathbf{J}_i)\rangle_{T,\mathbf{H}}. \tag{7}$$

In expression (7) we introduced the notation of [14]: B^γ and C_0^γ denote the magnetoelastic coefficient and the elastic constant without magnetic interactions, respectively. N is the number of rare-earth ions in the magnetic unit cell.

Using the molecular-field state calculated for several values of temperature T and magnetic field H by the *McPhase* program, the distortion was evaluated from equation (7). The calculated field dependence of $\sum_i \langle O_2^2(\mathbf{J}_i)\rangle_{T,\mathbf{H}}$ at $T = 2.5$ K is specifically shown in figure 4 (upper graph). It shows maxima at the metamagnetic transitions at about $\mu_0 H = 1$ and 2 T corresponding to the F2/F1 and F2/F phase boundaries. Note that there is no phase boundary at the minimum of $\sum_i \langle O_2^2(\mathbf{J}_i)\rangle$. (The magnetostriction curves in figures 1(b), (d) and 2(b), (d) have been interpreted accordingly.)

The result of the model calculation can be compared to the experimental data. For magnetic fields parallel to [0 1 0] the distortion can be estimated from

$$\varepsilon^\gamma = \frac{1}{\sqrt{2}}(\varepsilon_{aa} - \varepsilon_{bb}) = \frac{1}{\sqrt{2}}(\lambda_\perp - \lambda_\parallel) = \left(\frac{a}{b} - 1\right). \tag{8}$$

First the magnetostriction values (see figures 2(b), (d)) were normalized to the paramagnetic state taking into account the zero-field expansion (figures 2(a), (c)). Then the absolute values of the difference $(\lambda_\perp - \lambda_\parallel)/\sqrt{2}$ at $T = 2.5$ K are available. The curve is also plotted in figure 4 (lower graph). This curve resembles qualitatively the calculation for magnetic fields above 0.8 T. The fact that the calculated magnetostriction below 0.8 T is smaller than the measured one is attributed to magnetic domain effects which are not included in our present analysis (in order to do that accurately, information on the field dependence of the domain distribution is required). As a result of the analysis, we also obtain the value of the magnetoelastic constant $B^\gamma/C_0^\gamma = -3 \times 10^{-5} < 0$. This means a sample expansion perpendicular to the magnetic moments (or parallel to $\boldsymbol{q}$) in the transversely ordered phase when a transverse magnetic field is applied. This result agrees with the behaviour in the paramagnetic state, where domain effects can be neglected: the magnetostriction curves at $T = 10$ K show $\Delta\lambda_\parallel < 0$ and $\Delta\lambda_\perp > 0$, which means also an expansion normal to the field (or moment) direction.

Magnetostriction measurements in borocarbides were reported only for $HoNi_2B_2C$ [17] and $DyNi_2B_2C$ [18]. Judging from the features of the reported magnetostriction curves together with their H–T phase diagrams, it is expected that our analysis could be easily extended to these two cases as well as to most of the other magnetic borocarbides.

5. Summary

In summary, thermal expansion and magnetostriction isotherms were used to investigate and map out the H–T-phase diagram of $ErNi_2B_2C$. The phase diagram obtained agrees quite satisfactorily with the reported phase diagrams [4–7], indicating that macroscopic magnetostriction techniques are well suited for probing the low-temperature magnetic properties of borocarbides. In particular, for $T_{WF} < T < T_N$, the magnetic stability of the various phases as well as the metamagnetic transformations among them are reasonably well accounted for within a mean-field treatment that assumes a magnetic Hamiltonian composed of a crystal field, an exchange, a Zeeman, and an elastic term. This treatment reproduces the various aspects of the experimental H–T phase diagram. Because the magnetoelastic constant is negative, an elongation occurs perpendicular to the direction of the magnetic moments in an external field. Our analysis reveals the importance of magnetoelastic coupling in the analysis of magnetic properties in general and the magnetic phase diagram in particular.

Acknowledgments

Financial support from the Deutsche Forschungsgemeinschaft (Sonderforschungsbereich 463) is acknowledged. MElM acknowledges a fruitful discussion with D Schmitt and partial financial support from Brazilian agencies CNPq and FAPERJ.

References

[1] Zarestky J, Stassis C, Goldman A I, Canfield P C, Dervenagas P, Cho B K and Johnston D C 1995 *Phys. Rev.* B **51** 678
[2] Sinha S K, Lynn J W, Grigereit T E, Hossain Z, Gupta L C, Nagarajan R and Godart C 1995 *Phys. Rev.* B **51** 681
[3] Lynn J W, Skanthakumar S, Huang Q, Sinha S K, Hossain Z, Gupta L C, Nagarajan R and Godart C 1997 *Phys. Rev.* B 6584
[4] Canfield P C, Bud'ko S L and Cho B K 1996 *Physica* C **262** 249
[5] Bud'ko S L and Canfield P C 2000 *Phys. Rev.* B **61** R14932
[6] Campbell A J, Paul D M and McIntyre G J 2000 *Solid State Commun.* **115** 213
[7] Kawano H, Takeya H, Yoshizawa H and Kadowski K 1999 *J. Phys. Chem. Solids* **60** 1053
[8] Detlefs C, Islam A H M Z, Gu T, Goldman A I, Stassis C, Canfield P C, Hill J P and Vogt T 1997 *Phys. Rev.* B **56** 7843
[9] Kreyssig A, Schneidewind A, Loewenhaupt M, Ritter C, Freudenberger J, Fuchs G and Müller K-H 2001 *Rare Earth Transition Metal Borocarbides (Nitrides): Superconducting, Magnetic and Normal State Properties* ed K-H Müller and V Narozhnyi (Dordrecht: Kluwer) pp 137–54
[10] Takeya H, Hirano T and Kadowski K 1996 *Physica* C **256** 220
[11] Takeya H, Kadowski K, Hirata K and Hirano T 1996 *J. Alloys Compounds* **245** 94
[12] El Massalami M, Rapp R E, Changas E F, Takeya H, Chaves C M and Flores J 2002 *J. Phys. Soc. Japan* **71** 582
[13] Rotter M, Müller H, Gratz E, Doerr M and Loewenhaupt M 1998 *Rev. Sci. Instrum.* **69** 2742
[14] Morin P and Schmitt D 1990 *Ferromagnetic Materials* vol 5, ed K H J Buschow and E P Wohlfarth (Amsterdam: Elsevier) pp 1–132
[15] Jensen J and Mackintosh A R 1991 *Rare Earth Magnetism* (Oxford: Clarendon)
[16] Gasser U, Allensbach P, Furrer A and Mulders A M 1998 *J. Alloys Compounds* **275–7** 587
[17] Oomi G, Tagayama T, Mitamura H, Goto T, Cho B K and Canfield P C 2001 *Physica* B **294–5** 229
[18] Sierks C, Doerr M, Kreyssig A, Loewenhaupt M, Peng Z Q and Winzer K 1999 *J. Magn. Magn. Mater.* **192** 473